Discover Oncology

Analysis

Pyroptosis drives tumor progression and immune evasion in Hepatocellular Carcinoma: a single-cell and spatial transcriptomic study

Siyu Tao[1] · **Yunhao Yang**[2]

Received: 9 October 2024 / Accepted: 17 April 2025
Published online: 20 May 2025
© The Author(s) 2025 OPEN

Abstract

Background Pyroptosis is a form of programmed cell death characterized by inflammasome activation and the release of inflammatory cytokines, which induce a strong immune response. Unlike apoptosis, pyroptosis can elicit potent immune stimulation, potentially playing a crucial role in anti-tumor immunity. However, it may also promote tumor progression by altering the tumor microenvironment and facilitating immune evasion. This study investigates pyroptosis-related gene expression in hepatocellular carcinoma (HCC), with a focus on identifying key genes that influence prognosis and tumor microenvironment dynamics.

Methods Single-cell RNA sequencing (scRNA-seq) data from 10 HCC patients were obtained from the GEO database (GSE149614), along with spatial transcriptomic data and bulk RNA-seq data from TCGA. We performed data processing and quality control using the Seurat package and applied machine learning techniques, including LASSO regression, to identify key pyroptosis-related genes. Functional analyses, including Gene Ontology (GO), KEGG, and GSVA, were conducted to explore biological pathways. Pyroptosis levels were quantified across cell types, and survival analysis was performed to evaluate prognostic impacts. Cell communication and immune infiltration were also assessed to understand the tumor microenvironment.

Results We identified CHMP4B as a key pyroptosis-related gene in HCC, significantly associated with poor prognosis. High CHMP4B expression was correlated with shorter overall survival (OS) and disease-free survival (DFS). Functional enrichment analysis showed that CHMP4B is involved in cell cycle regulation, DNA repair, and cytoskeletal organization. Spatial transcriptomics revealed heterogeneous CHMP4B expression in the tumor microenvironment, with higher levels found in advanced tumor stages. Moreover, high CHMP4B expression was associated with increased infiltration of immunosuppressive cells, such as monocytes and macrophages, and upregulation of immune checkpoint molecules (PD-L1, CTLA4), suggesting its role in promoting immune evasion.

Conclusions Our findings highlight CHMP4B as a critical regulator of pyroptosis in HCC, influencing tumor progression and immune modulation. High CHMP4B expression may facilitate the development of an immunosuppressive microenvironment, enabling immune escape and tumor growth. The study underscores CHMP4B's potential as a prognostic biomarker and therapeutic target in HCC. However, the limited sample size calls for further validation using larger datasets and multi-omics approaches, such as proteomics and metabolomics, to fully elucidate its functional role in HCC pathogenesis.

Keywords Pyroptosis · Hepatocellular Carcinoma · Single-Cell · Spatial Transcriptomic Study · Bioinformatics

✉ Siyu Tao, 15213227714@163.com | [1]Department of Laboratory Medicine, Daping Hospital, Army Medical Center of PLA, Chongqing, China 400042. [2]The First Clinical Medical College, Chongqing Medical University, Chongqing, China.

1 Introduction

Liver cancer is one of the most common malignancies worldwide, with particularly high incidence rates in East Asia and Africa. According to the latest statistics, approximately 900,000 new cases of liver cancer are diagnosed globally each year, making it a leading cause of cancer-related mortality [1–4]. The primary etiologies of liver cancer include chronic hepatitis B virus (HBV) and hepatitis C virus (HCV) infections, alcoholic liver disease, non-alcoholic fatty liver disease (NAFLD), and cirrhosis. Additionally, genetic factors, environmental influences, and lifestyle choices may contribute to the development of liver cancer. [5]Symptoms of liver cancer include upper abdominal pain, jaundice, and loss of appetite. Common diagnostic methods include imaging techniques (such as CT and MRI), serum biomarkers (such as alpha-fetoprotein [AFP]), and liver biopsy. Treatment options for liver cancer range from surgical resection and liver transplantation to locoregional therapies (such as radiofrequency ablation and transarterial chemoembolization) and systemic therapies (such as targeted drugs and immunotherapy) [4, 6, 7].

Pyroptosis is a form of programmed cell death closely linked to inflammatory responses. Its mechanisms involve inflammasome activation (e.g., NLRP3 inflammasome), caspase-1 activation, and the release of gasdermins and inflammatory cytokines, such as IL-1β and IL-18 [8]. Unlike apoptosis (which is characterized by a self-destructive process within the cell) and autophagy (which involves the degradation of intracellular components for cell survival or death), pyroptosis is distinguished by noticeable cell membrane rupture and robust inflammatory responses. Research has shown that pyroptosis plays a pivotal role in the development and progression of liver cancer. It not only impacts the survival of liver cancer cells but also drives changes in the tumor microenvironment by releasing inflammatory mediators, which facilitate immune evasion and metastasis [9]. Dysregulated expression of pyroptosis-related genes (such as NLRP3, caspase-1, and IL-1β) is closely linked to the onset and progression of liver cancer and is associated with poor prognosis [10, 11].

Single-cell sequencing technology enables the analysis of gene expression at the single-cell level, offering insights into cellular heterogeneity and specific gene expression patterns. Compared to traditional bulk cell analysis, single-cell techniques provide higher-resolution data, allowing for the discovery of differences between cell populations [12]. Current research has primarily focused on the overall role of pyroptosis in liver cancer and its interactions with other forms of cell death. However, detailed investigations at the single-cell level remain limited. [13] Analyzing the single-cell expression profiles of pyroptosis-related genes in liver cancer could offer new insights into the mechanisms through which pyroptosis contributes to tumor development. This research may also identify novel molecular targets for early diagnosis and personalized therapies, ultimately enhancing patient prognosis and quality of life.

2 Materials and Methods

2.1 Data Sources

The single-cell RNA sequencing data used in this study were obtained from the GEO dataset GSE149614, which includes sequencing data from 10 HCC patients. We selected two types of samples for analysis: primary tumor tissues and non-tumorous liver tissues. Additionally, spatial transcriptomics data of HCC tumor tissue were obtained from GSM6177612, which was derived from a tumor region of primary hepatocellular carcinoma. RNA-seq data for HCC were also downloaded from the UCSC Xena platform (https://xena.ucsc.edu/), specifically from the TCGA (The Cancer Genome Atlas) cohort, comprising sequencing information from 424 samples, along with corresponding survival data for survival analysis. External validation datasets GSE144269, GSE76427, and ICGC_LIRI were also utilized.

2.2 Single-Cell Sequencing Data Processing and Cell Type Identification

After retrieving single-cell sequencing data from 10 tumor samples and 8 normal liver samples, we performed initial processing using the Seurat package, including quality control, dimensionality reduction, clustering, and visualization. To ensure the reliability of the sequencing data for further analysis, strict quality control measures were applied: cells with fewer than 500 or more than 6,000 detected genes, as well as cells with mitochondrial gene content exceeding 20%, were removed to eliminate empty droplets, doublets, and senescent cells. After normalizing and scaling the data, principal component analysis (PCA) was performed for dimensionality reduction. To correct for batch effects, the"harmony"package was applied. Clustering was conducted using the top 20 principal components with a resolution of 0.3, resulting in 17

cell clusters. Visualization was achieved via UMAP. Preliminary cell type identification was conducted using known cell markers and the"FindAllMarkers"function [14].

2.3 Tumor Cell Identification

Tumor cells were identified using the"copykat"package to analyze copy number variations (CNVs). CopyKAT (Copynumber Karyotyping of Tumors) is a computational tool that integrates Bayesian methods to identify genome-wide aneuploidy in single cells at a 5MB resolution, distinguishing tumor cells from normal cells. Cells with widespread genome-wide CNV aberrations (aneuploidy) were classified as tumor cells, while stromal cells and immune cells typically displayed diploid (2 N) or near-diploid copy number profiles [15].

2.4 Pyroptosis Level Assessment

To quantify pyroptosis levels in different cell types, we utilized a gene set of 52 pyroptosis-related genes and applied multiple gene set scoring methods, including AddModuleScore, ssGSEA, AUCell, UCell, and singscore. Each method generated a score for each cell, which was then centralized and standardized. The final score for each cell was obtained by summing the standardized scores from all five methods. Using multiple scoring approaches reduced error and bias, providing more comprehensive and robust biological insights. Cells were divided into high- and low-score groups based on the median score, representing cells with different levels of pyroptosis.

2.5 Enrichment Analysis and Cell–Cell Communication Analysis

To explore the biological functional differences between cells with high and low pyroptosis levels, we performed Gene Ontology (GO) and KEGG pathway enrichment analysis. The genes used for enrichment were identified by the"FindMarkers"function, which highlights genes upregulated in high-score cells. Enrichment analysis was performed using the"clusterProfiler"package, and the results were visualized accordingly. The"GSVA"package was also used, applying the"HALLMARK"gene sets to identify tumor-related biological processes. For cell–cell communication analysis, we used the"CellChat"package to simulate and analyze cell signaling networks. CellChat considers gene expression data and known interactions between signaling ligands, receptors, and co-factors to model intercellular communication [16].

2.6 Patient Infiltration and Prognosis Analysis Based on High- and Low-Score Cells

To evaluate patient immune infiltration based on high- and low-score pyroptotic cells, we identified marker genes of these cells and performed ssGSEA scoring on TCGA data. Patients were classified into high- and low-infiltration groups, and Kaplan–Meier (K-M) survival curves were plotted to compare survival differences. The"survival"and"survminer"packages were used to generate K-M curves for overall survival, progression-free survival, disease-free survival, and disease-specific survival [16].

2.7 Spatial Transcriptomics Deconvolution Analysis

Spatial transcriptomics data were processed using the"Seurat"package, with mitochondrial and ribosomal genes excluded during quality control, while preserving data from all spots. Data were normalized using the"SCTransform"function and PCA was applied for dimensionality reduction, followed by clustering based on the top 20 principal components, yielding seven cell clusters. The"scMetabolism"package was used to infer metabolic activity for each cell cluster within the spatial transcriptomics data, employing built-in gene sets covering 85 KEGG pathways and 82 Reactome terms, using the VISION algorithm for scoring. To overcome the resolution limitations of spatial transcriptomics and fully leverage spatial information, we applied deconvolution analysis using the"spacexr"package for RCTD deconvolution. Annotated single-cell data were used for deconvolution of spatial transcriptomics, allowing for the inference of cell type probabilities for each sequencing spot. Cells with high- and low-pyroptosis scores were also included in the analysis to compare pyroptosis levels across spatial regions [17].

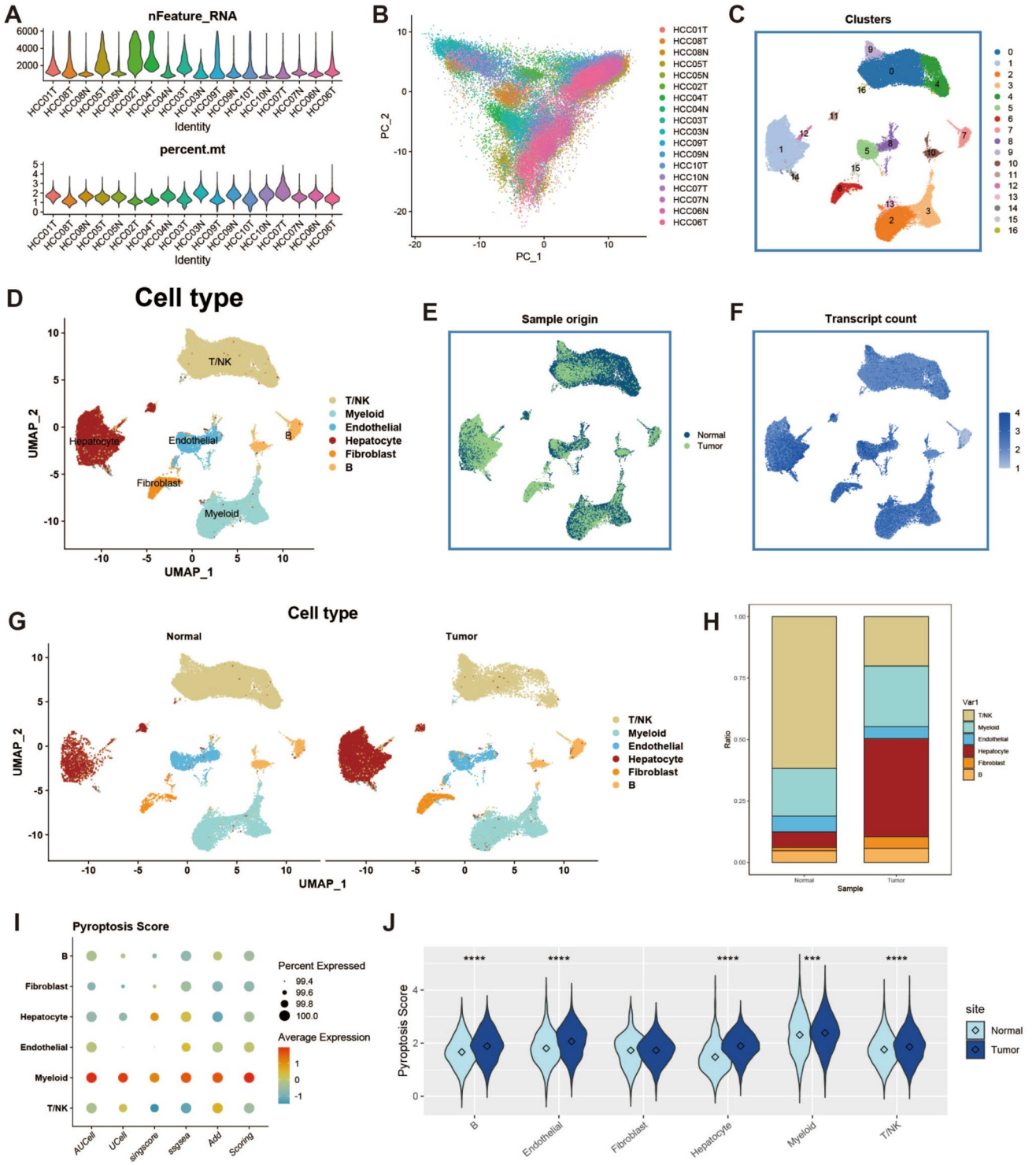

Fig. 1 Cell type identification and pyroptosis level assessment.**A**: Violin plot showing sample characteristics after quality control of single-cell data, with the top chart showing the number of detected genes and the bottom chart showing the proportion of mitochondrial genes.**B**: PCA plot showing cell distribution across different samples after removing batch effects.**C**: UMAP of clustered cell groups after dimensionality reduction, showing 17 groups.**D**: Results of cell type identification.**E**: UMAP showing the distribution of cells in different groups.**F**: Heatmap of cell count values.**G**: Display of cell type identification results, showing the distribution and number of each cell type in different groups.**H**: Bar plot showing cell proportions.**I**: Bubble chart of gene set scoring results.**J**: Violin plot of differential score analysis between tumor and normal group cells

2.8 Expression and Prognosis Analysis of Key Pyroptosis-Related Genes

Differential expression analysis of key pyroptosis-related genes was performed using TCGA data, and results were validated using GEO data. Six significantly differentially expressed pyroptosis-related genes were then used to score bulk RNA-seq data, dividing patients into high- and low-score groups for survival analysis. ssGSEA was employed for scoring, and Kaplan–Meier curves were plotted to compare the prognostic impact of these genes. External datasets from GEO and ICGC were also used for validation. In the spatial transcriptomics data, we analyzed the expression of key pyroptosis genes, comparing expression levels across normal cells, mixed cells, and malignant cell regions, and assessed correlations with various cell types. To further filter genes with prognostic significance in liver cancer, Lasso regression was performed using the glmnet package with ten-fold cross-validation, selecting the optimal model coefficients and genes.

2.9 Prognostic and Clinical Correlation Analysis of CHMP4B

For the key pyroptosis gene CHMP4B, we performed subgroup differential expression analysis using clinical information from TCGA. Prognostic value of CHMP4B was assessed using TCGA and external validation datasets. Enrichment analysis, immune infiltration analysis, and spatial transcriptomics data were also incorporated into the study of CHMP4B.

2.10 Cell Culture and Transient Transfection

The human hepatocellular carcinoma cell lines HepG2 and Huh7 (GeneChem, Shanghai) were cultured in high-glucose DMEM medium (Gibco) supplemented with 10% fetal bovine serum (FBS, Gibco), 100 U/mL penicillin, and 100 µg/mL streptomycin (Thermo Fisher Scientific). All cells were maintained in a humidified incubator at 37 °C with 5% CO_2 (Thermo Forma) and the medium was changed regularly to maintain cell viability.

For transient transfection experiments, cells were seeded in 6-well plates at a confluence of 50%–70%. After 24 h of cell attachment, siRNA or overexpression plasmid transfections were performed using Lipofectamine 3000 transfection reagent (Invitrogen). Cells were collected 48 h post-transfection for subsequent experiments.

2.11 Quantitative Real-Time PCR (qRT-PCR)

To determine the mRNA expression levels of CHMP4B in hepatocellular carcinoma cells, total RNA was extracted from HepG2 and Huh7 cells using TRIzol reagent (Invitrogen) according to the manufacturer's instructions. RNA quality was assessed using a NanoDrop 2000 (Thermo Fisher Scientific) to ensure an A260/A280 ratio between 1.8 and 2.0. The RNA was reverse-transcribed into cDNA using PrimeScript RT Master Mix (Takara). Subsequently, qRT-PCR was performed on an ABI 7500 Real-Time PCR system. The PCR reaction mixture had a total volume of 20 µL, containing 10 µL of SYBR Green Master Mix (Takara), 1 µL of cDNA template, 0.5 µL of forward primer for CHMP4B (10 µM), 0.5 µL of reverse primer for CHMP4B (10 µM), and 8 µL of RNase-free water. The PCR conditions were as follows: initial denaturation at 95 °C for 30 s, followed by 40 cycles of denaturation at 95 °C for 5 s and annealing/extension at 60 °C for 30 s. GAPDH was used as the internal reference gene. The primer sequences were as follows: CHMP4B forward primer: 5′-AGTCCCTGACAGCTTCTCCG-3′; CHMP4B reverse primer: 5′-CTGGTGCTTTGATGTCCTGGA-3′. The relative expression levels were calculated using the 2^-ΔΔCt method and subjected to statistical analysis.

2.12 Statistical Analysis

Statistical analyses were conducted using R 4.2.2 and its associated packages. For continuous variables, the non-parametric Wilcoxon rank-sum test was used to assess relationships between groups. Spearman correlationanalysis was used to test correlation coefficients. A significance threshold of $P < 0.05$ was set for all statistical analyses.

Fig. 2 Hepatocyte analysis.**A**: UMAP of cells with high and low scores, with red representing high pyroptosis level cells and green representing low pyroptosis level cells.**B**: Bar plot of cell proportions.**C**: Divergent bar chart of GSVA enrichment results for Hallmark gene sets, with pathways enriched in low-score cells on the left and pathways enriched in high-score cells on the right.**D**: Bar chart of GO enrichment analysis results.**E**: Bar chart of KEGG enrichment analysis results.**F**: Bar plot comparing communication frequency and intensity.**G**: Bar plot comparing communication pathways.**H**: Heatmap of communication pathway intensity.**I**: Scatter plot showing signal reception and transmission intensities of cells.**J**: UMAP showing copy number variation, with red indicating polyploid cells (i.e., tumor cells).**K**: GSEA enrichment results for KEGG gene sets, with nucleotide metabolism on top and ribosome on the bottom.**L**: Bar plot showing cell proportions, with malignant cells on the left and non-malignant cells on the right.**M**: KM curves of overall survival, disease-specific survival, disease-free survival, and progression-free survival in high- and low-infiltration groups.**N**: Violin plot showing differential expression of pyroptosis-related genes in hepatocytes

3 Result

3.1 Single-Cell Quality Control

In this study, we obtained single-cell transcriptomic data from the GEO database (dataset GSE149614). Initially, we performed data quality control on all single-cell samples. To eliminate the influence of senescent cells, red blood cells, and cells with high mitochondrial content, we quantified relevant quality metrics, including UMI counts and the percentage of mitochondrial and hemoglobin gene expression (Fig. 1A). Batch effects were removed using the Harmony package to ensure that observed differences were purely biological in nature (Fig. 1B). After dimensionality reduction and clustering, a total of 61,776 cells passed quality control and were clustered into 16 groups, which were visualized using UMAP (Fig. 1C). Cell clusters were named based on marker gene expression and upregulated genes (Fig. 1D), with tumor and normal groups showing distinct distribution patterns (Fig. 1E), as well as mRNA density differences (Fig. 1F).

The distribution of all cell types in the tumor and normal groups is shown (Fig. 1G, H), with a bar chart indicating a significant decrease in immune cell content and an increase in hepatocyte proportions in the tumor group. To identify pyroptosis-related cell clusters, we scored all cells based on pyroptosis-related gene expression and compared differences between normal and tumor samples (Fig. 1I, J). The results indicated significant variations in pyroptosis levels.

3.2 Pyroptosis Characteristics in Hepatocytes within the Tumor Microenvironment

Hepatocytes are the main component of the liver cancer tumor microenvironment. We divided hepatocytes into high and low pyroptosis score groups (Fig. 2A) and found that hepatocytes in the tumor group exhibited higher pyroptosis characteristics compared to the normal group (Fig. 2B). To explore heterogeneity between the two groups, we performed a GSVA analysis to identify functional differences between high and low pyroptosis score hepatocytes (Fig. 2C).

GO enrichment analysis revealed that high pyroptosis score hepatocytes showed increased levels of programmed cell death and vacuole fusion (Fig. 2D). KEGG pathway analysis indicated that these hepatocytes were more active in thyroid cancer and Salmonella infection pathways (Fig. 2E). In terms of cell communication, we assessed the intensity of communication and receptor-ligand interactions, showing higher communication scores in the high pyroptosis group (Fig. 2F). Additionally, we evaluated the input–output signaling of cell communication, finding that high pyroptosis hepatocytes had more robust communication and signal output characteristics (Fig. 2G, H, I).

Figure 2J displays a group of highly aberrant cells identified via the copykat method, which we classified as cancer cells. Further KEGG enrichment analysis of cancer cells with varying pyroptosis levels revealed that nucleotide metabolism and ribosome pathways were enriched with the most differential genes (Fig. 2K). A subsequent analysis of cell proportions indicated that pyroptosis features were more pronounced in tumor cells (Fig. 2L). Survival curves showed that patients with high pyroptosis levels had shorter overall survival (OS) and progression-free survival (PFS) compared to those with lower pyroptosis (Fig. 2M). To further explore the prognostic impact of pyroptosis in liver cancer, we analyzed pyroptosis gene expression levels, revealing that most pyroptosis-related genes were upregulated in tumor tissues (Fig. 2N).

survival, disease-free survival, and progression-free survival in high- and low-infiltration groups.N: Violin plot showing differential expression of pyroptosis-related genes in hepatocytes.

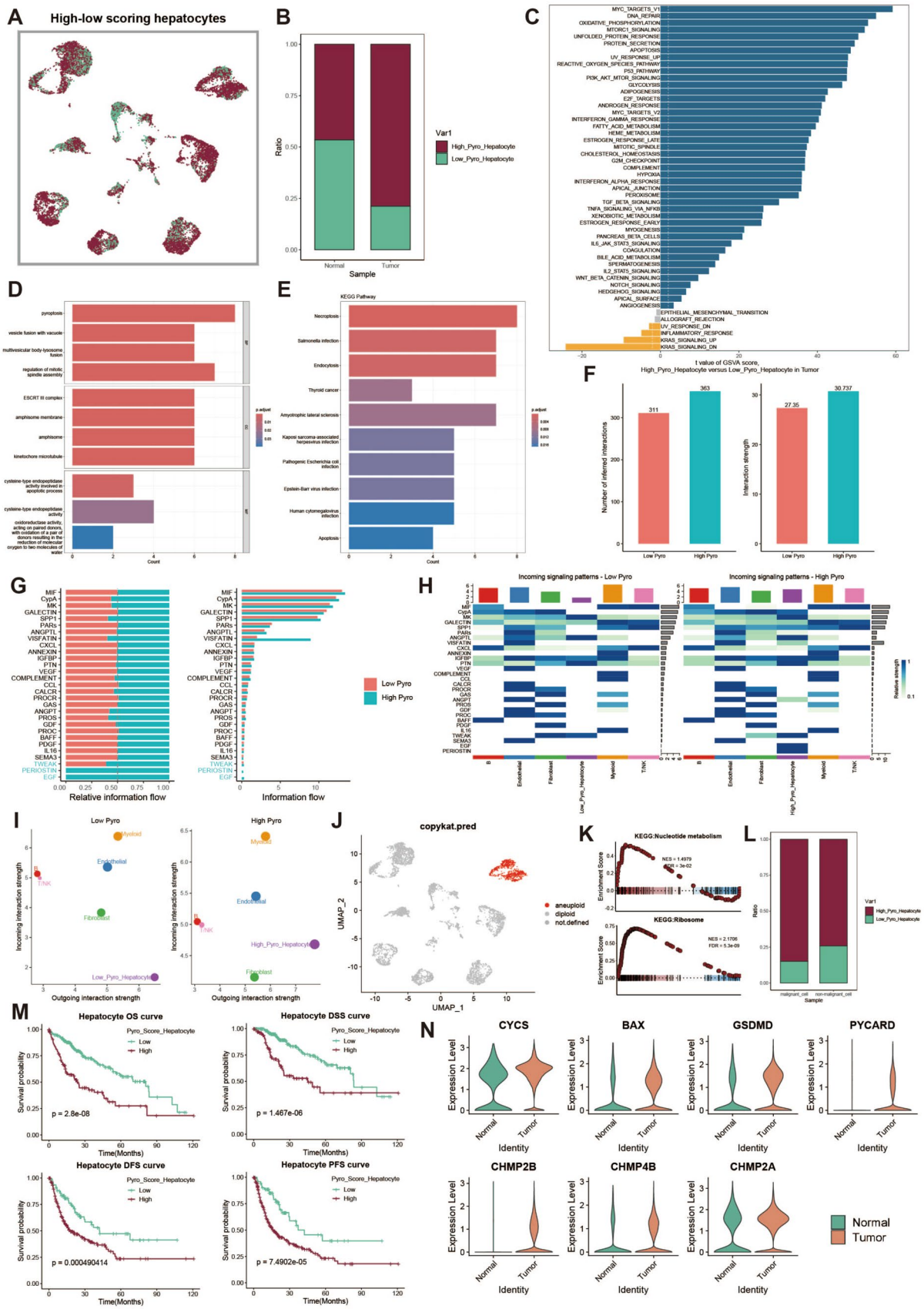
A
High-low scoring hepatocytes
B
Ratio
Sample
Normal
Tumor
Var1
High_Pyro_Hepatocyte
Low_Pyro_Hepatocyte
C
MYC_TARGETS_V1
DNA_REPAIR
OXIDATIVE_PHOSPHORYLATION
MTORC1_SIGNALING
UNFOLDED_PROTEIN_RESPONSE
PROTEIN_SECRETION
APOPTOSIS
UV_RESPONSE_UP
REACTIVE_OXYGEN_SPECIES_PATHWAY
P53_PATHWAY
PI3K_AKT_MTOR_SIGNALING
GLYCOLYSIS
ADIPOGENESIS
E2F_TARGETS
ANDROGEN_RESPONSE
MYC_TARGETS_V2
INTERFERON_GAMMA_RESPONSE
FATTY_ACID_METABOLISM
HEME_METABOLISM
ESTROGEN_RESPONSE_LATE
MITOTIC_SPINDLE
CHOLESTEROL_HOMEOSTASIS
G2M_CHECKPOINT
COMPLEMENT
HYPOXIA
INTERFERON_ALPHA_RESPONSE
APICAL_JUNCTION
PEROXISOME
TGF_BETA_SIGNALING
TNFA_SIGNALING_VIA_NFKB
XENOBIOTIC_METABOLISM
ESTROGEN_RESPONSE_EARLY
MYOGENESIS
PANCREAS_BETA_CELLS
IL6_JAK_STAT3_SIGNALING
COAGULATION
BILE_ACID_METABOLISM
SPERMATOGENESIS
IL2_STAT5_SIGNALING
WNT_BETA_CATENIN_SIGNALING
NOTCH_SIGNALING
HEDGEHOG_SIGNALING
APICAL_SURFACE
ANGIOGENESIS
EPITHELIAL_MESENCHYMAL_TRANSITION
ALLOGRAFT_REJECTION
UV_RESPONSE_DN
INFLAMMATORY_RESPONSE
KRAS_SIGNALING_UP
KRAS_SIGNALING_DN
t value of GSVA score,
High_Pyro_Hepatocyte versus Low_Pyro_Hepatocyte in Tumor
D
pyroptosis
vesicle fusion with vacuole
multivesicular body-lysosome fusion
regulation of mitotic spindle assembly
ESCRT III complex
amphisome membrane
amphisome
kinetochore microtubule
cysteine-type endopeptidase activity involved in apoptotic process
cysteine-type endopeptidase activity
oxidoreductase activity, acting on paired donors, with oxidation of a pair of donors resulting in the reduction of molecular oxygen to two molecules of water
p.adjust
Count
E
KEGG Pathway
Necroptosis
Salmonella infection
Endocytosis
Thyroid cancer
Amyotrophic lateral sclerosis
Kaposi sarcoma-associated herpesvirus infection
Pathogenic Escherichia coli infection
Epstein-Barr virus infection
Human cytomegalovirus infection
Apoptosis
F
Number of inferred interactions
Interaction strength
311
363
27.35
30.737
Low Pyro
High Pyro
G
Relative information flow
Information flow
Low Pyro
High Pyro
H
Incoming signaling patterns - Low Pyro
Incoming signaling patterns - High Pyro
Relative strength
I
Low Pyro
High Pyro
Incoming interaction strength
Outgoing interaction strength
Myeloid
Endothelial
Fibroblast
B
T/NK
High_Pyro_Hepatocyte
Low_Pyro_Hepatocyte
J
copykat.pred
aneuploid
diploid
not.defined
UMAP_1
UMAP_2
K
KEGG:Nucleotide metabolism
KEGG:Ribosome
Enrichment Score
NES = 1.4979
FDR = 3e-02
NES = 2.1706
FDR = 5.3e-09
L
Ratio
Sample
malignant_cell
non-malignant_cell
Var1
High_Pyro_Hepatocyte
Low_Pyro_Hepatocyte
M
Hepatocyte OS curve
Hepatocyte DSS curve
Hepatocyte DFS curve
Hepatocyte PFS curve
Pyro_Score_Hepatocyte
Low
High
Survival probability
Time(Months)
p = 2.8e-08
p = 1.467e-06
p = 0.000490414
p = 7.4902e-05
N
CYCS
BAX
GSDMD
PYCARD
CHMP2B
CHMP4B
CHMP2A
Expression Level
Identity
Normal
Tumor

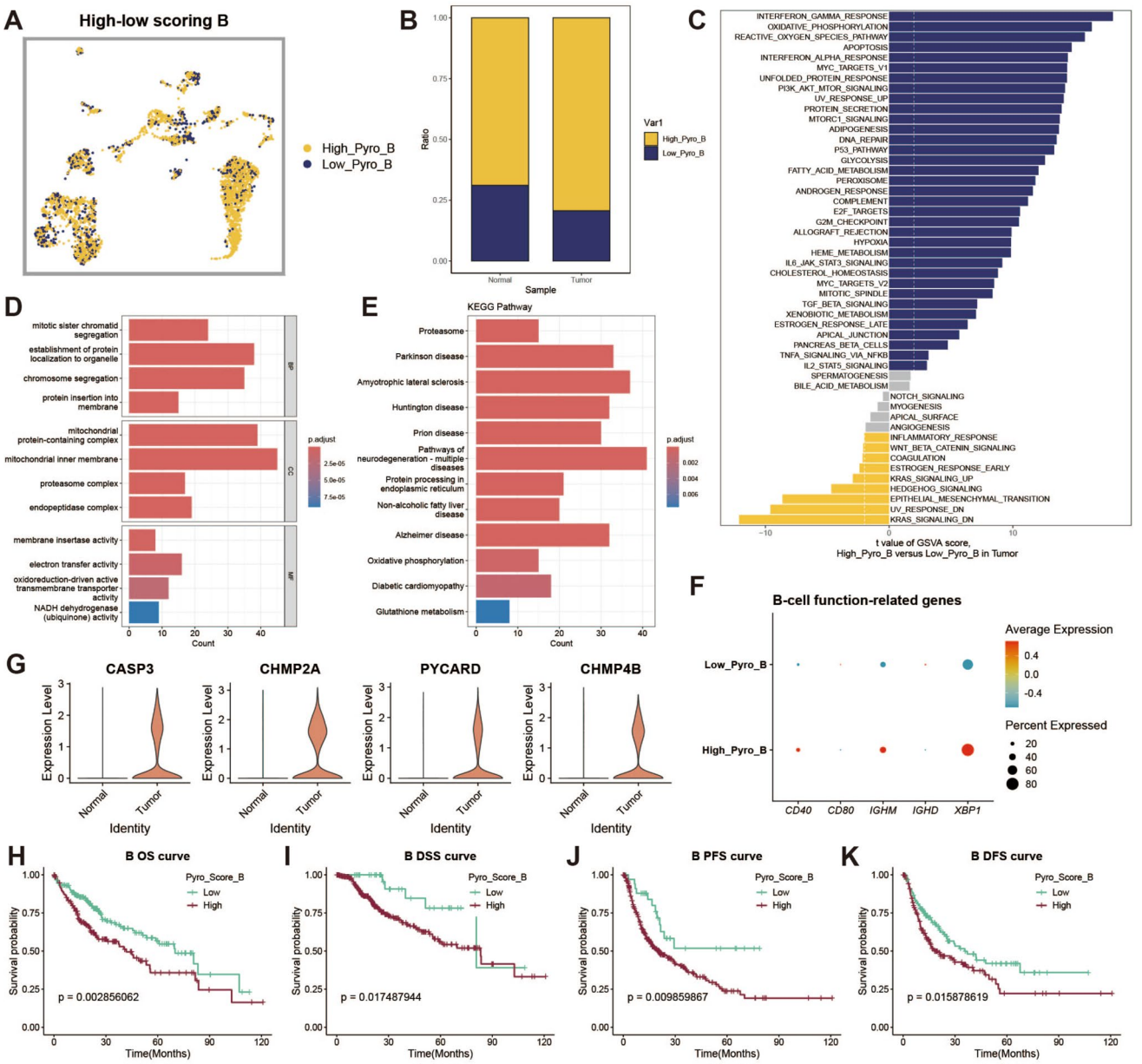

Fig. 3 B cell analysis.**A**: UMAP of cells with high and low scores, with yellow representing high pyroptosis level cells and blue representing low pyroptosis level cells.**B**: Bar plot of cell proportions.**C**: Divergent bar chart of GSVA enrichment results for Hallmark gene sets, with pathways enriched in low-score cells on the left and pathways enriched in high-score cells on the right.**D**: Bar chart of GO enrichment analysis results.**E**: Bar chart of KEGG enrichment analysis results.**F**: Bubble chart showing expression levels of genes related to B cell functions.**G**: Violin plot showing differential expression of pyroptosis-related genes in B cells.**H–K**: KM curves of overall survival, disease-specific survival, disease-free survival, and progression-free survival in patients with high and low infiltration

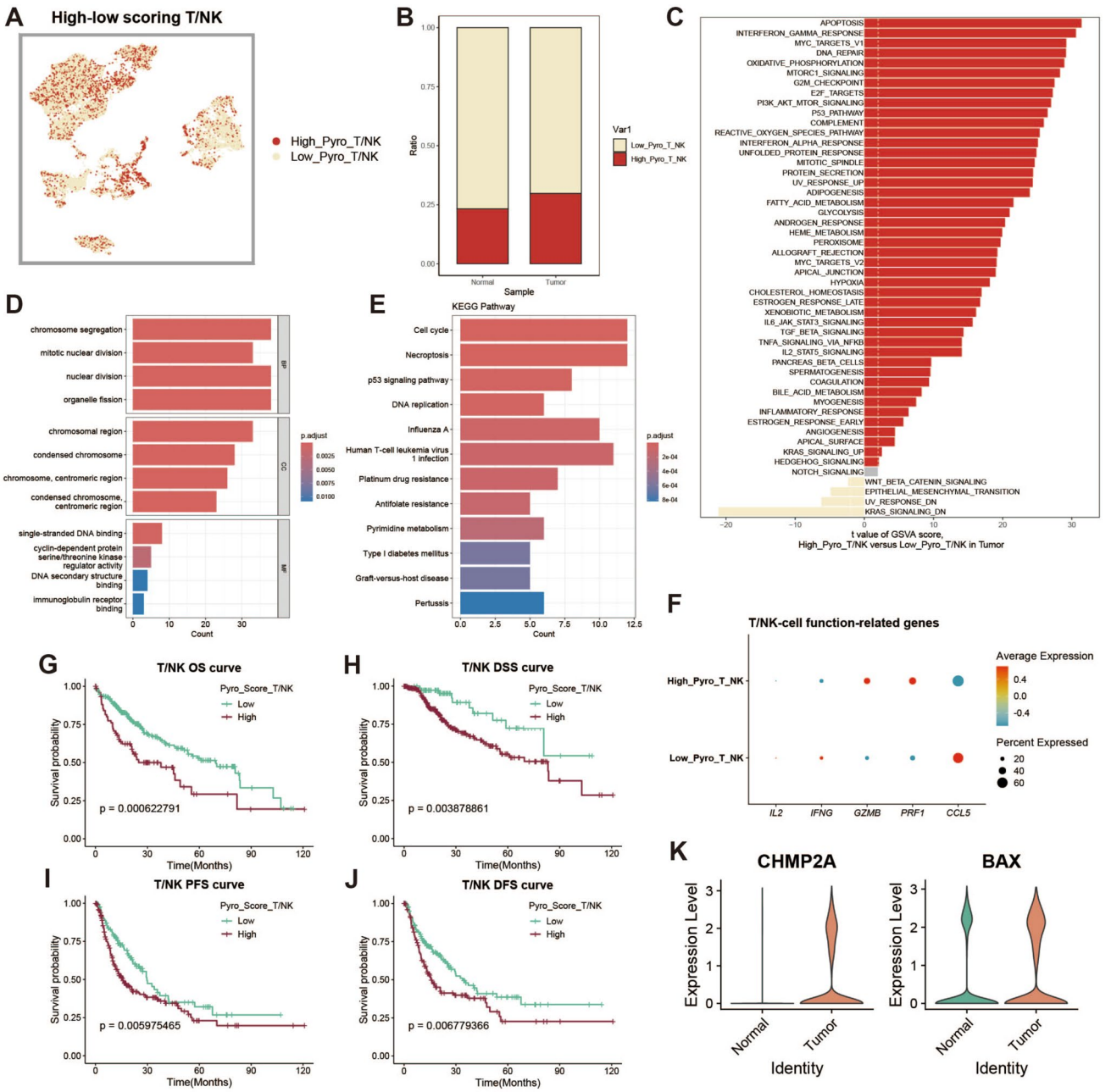

Fig. 4 T/NK cell analysis.**A**: UMAP of cells with high and low scores, with red representing high pyroptosis level cells and yellow representing low pyroptosis level cells.**B**: Bar plot of cell proportions.**C**: Divergent bar chart of GSVA enrichment results for Hallmark gene sets, with pathways enriched in low-score cells on the left and pathways enriched in high-score cells on the right.**D**: Bar chart of GO enrichment analysis results.**E**: Bar chart of KEGG enrichment analysis results.**F**: Bubble chart showing expression levels of genes related to T/NK cell functions.**G-J**: KM curves of overall survival, disease-specific survival, disease-free survival, and progression-free survival in patients with high and low infiltration.**K**: Violin plot showing differential expression of pyroptosis-related genes in T/NK cells

3.3 Pyroptosis Characteristics of B Cells in the Tumor Microenvironment

To explore pyroptosis characteristics in B cells within the liver cancer tumor microenvironment, we divided B cells into high and low pyroptosis score groups (Fig. 3A). B cells in the tumor group exhibited higher pyroptosis levels compared to the normal group (Fig. 3B). To investigate the heterogeneity between the two groups, we performed a GSVA analysis to examine functional differences between high and low pyroptosis B cells (Fig. 3C).

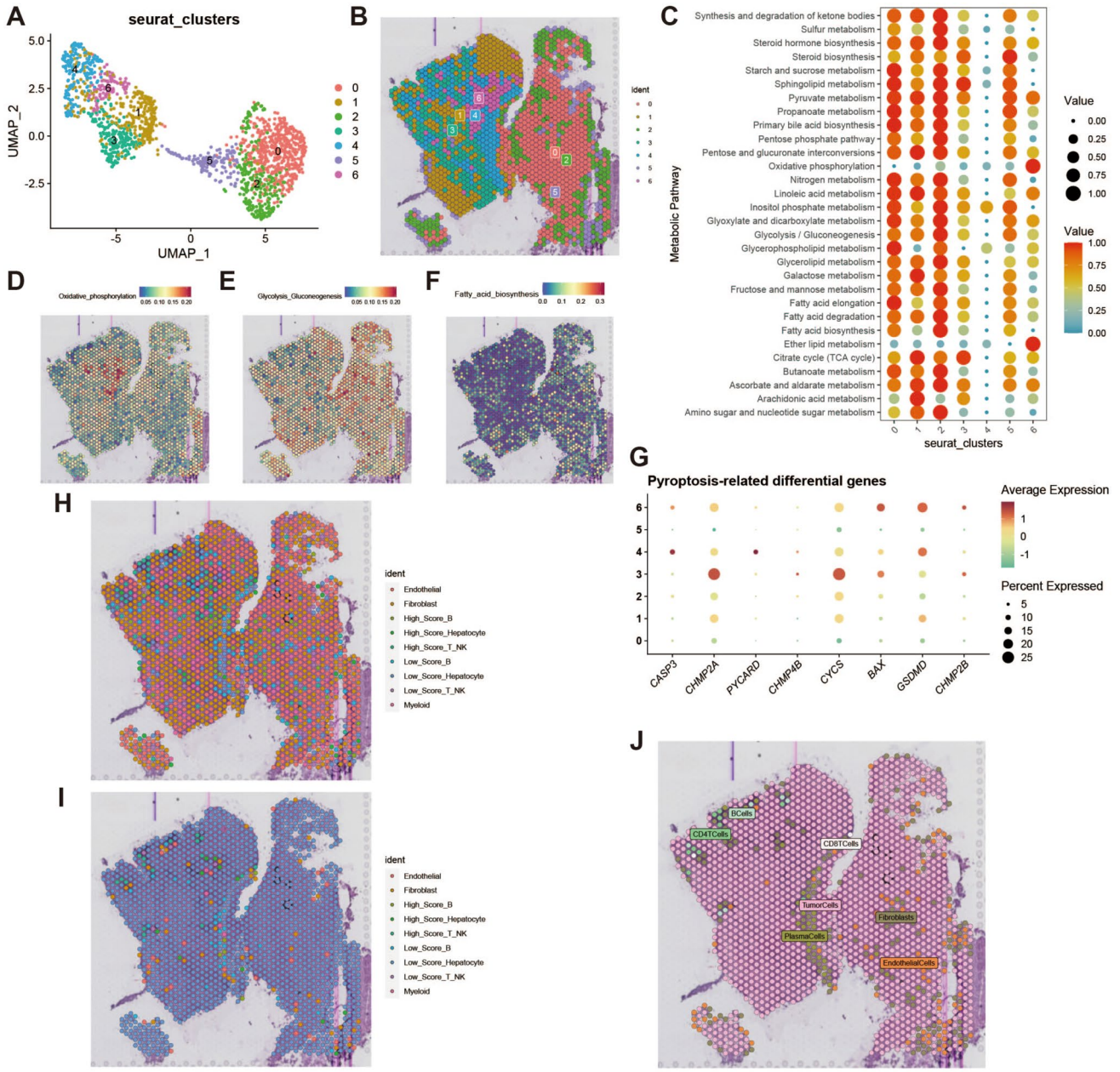

Fig. 5 Spatial transcriptomic metabolic analysis and deconvolution analysis.**A**: UMAP of clustering results after dimensionality reduction.**B**: Dimensionality reduction clustering plot of spatial transcriptomic slices.**C**: Bubble chart of metabolic pathway activity intensity.**D-F**: Heatmaps of oxidative phosphorylation, glycolysis, and fatty acid metabolism intensities.**G**: Bubble chart showing expression levels of key pyroptosis-related genes in spatial transcriptomic data.**H**: Deconvolution analysis incorporating high and low pyroptosis levels, showing the primary probability of cell types.**I**: Deconvolution analysis incorporating high and low pyroptosis levels, showing the secondary probability of cell types.**J**: Image showing the most probable cell type for each spot based on cell type probability

High pyroptosis score B cells showed enhanced protein localization and regulation of protein secretion (Fig. 3D, E). To assess the functional impact of different pyroptosis levels in B cells, we compared functional gene expression across various pyroptosis scores (Fig. 3F). Additionally, we analyzed pyroptosis gene expression levels in liver cancer tissues, revealing that most genes were upregulated in tumor tissues (Fig. 3G). Survival curves indicated that patients with high pyroptosis B cells had shorter OS and PFS compared to the low-pyroptosis group (Fig. 3H-K).

3.4 Pyroptosis Characteristics of T/NK Cells in the Tumor Microenvironment

T/NK cells play a critical role in the immune system by recognizing and eliminating pathogens, virus-infected cells, and tumor cells. We divided T/NK cells into high and low pyroptosis score groups. T/NK cells in the tumor group exhibited higher pyroptosis characteristics compared to the normal group (Fig. 4A, B). To explore functional differences between the two groups, we conducted a GSVA analysis (Fig. 4C), which showed significant upregulation of pathways related to oxidative stress and immune responses in the high pyroptosis group.

GO and KEGG enrichment analyses (Figs. 4D, E) revealed that T/NK cells with high pyroptosis scores were significantly enriched in pathways related to cell cycle regulation, p53 signaling, and DNA replication. Immune-killing-related genes were more highly expressed in the high-pyroptosis group (Fig. 4F), where patients with high pyroptosis T/NK cells exhibited poorer prognosis. Several pyroptosis-related functional genes, such as CHMP2 A and BAX, showed significant expression differences between normal and tumor tissues (Fig. 4G), suggesting that pyroptosis may play a crucial role in tumor progression. Survival analysis revealed significant differences in OS, DSS, PFS, and DFS between patients with high and low pyroptosis T/NK cells (Figs. 4H-K).

3.5 Spatial Transcriptomic Analysis of Pyroptosis Characteristics

To further investigate pyroptosis characteristics in liver cancer, we conducted deconvolution analysis on spatial transcriptomic data. Spatial transcriptomic sequencing data of HCC tumor tissue were downloaded from GSM6177612, with the tissue slices originating from primary hepatocellular carcinoma. After dimensionality reduction and clustering, seven cell clusters were visualized using UMAP (Fig. 5A). Spatial distribution of all cell clusters is shown in Fig. 5B.

Metabolic differences were assessed for each cluster, showing higher metabolic activity in clusters 0, 1, and 2 (Fig. 5C). We also analyzed the spatial levels of glycolysis and oxidative phosphorylation pathways in different regions (Fig. 5D-F). Furthermore, pyroptosis-related gene scoring was performed at the spatial level (Fig. 5G), and deconvolution analysis projected single-cell annotations onto spatial spots (Fig. 5H, I), displaying the primary and secondary probabilities of different pyroptosis levels for each spot (Fig. 5J).

3.6 Transcriptomic Analysis of Key Pyroptosis Genes

Differential expression analysis of key pyroptosis genes between tumor and normal samples was conducted using TCGA and GEO data (Fig. 6A). ssGSEA scoring indicated elevated pyroptosis levels in tumor samples compared to normal tissues (Fig. 6B, G, H). To refine the impact of pyroptosis at different tumor stages, we also analyzed and displayed pyroptosis score differences among patients at different clinical stages (Fig. 6C-F).

In spatial transcriptomic data, malignant cells, mixed cells, and normal cells were identified, with the pyroptosis scores of each cell type shown (Fig. 6I). By analyzing the Spearman correlation between pyroptosis-related gene AUC scores and microenvironmental components, we further confirmed the key role of pyroptosis in liver cancer (Fig. 6J). GO enrichment analysis of high- and low-pyroptosis score patients revealed potential factors influencing prognosis (Fig. 6K, L).

3.7 Machine Learning Identification of Prognostic Genes

Using machine learning, we identified pyroptosis-related genes that influence prognosis and survival in liver cancer patients. The LASSO regression model identified key genes such as CHMP2 A and CHMP4B (Fig. 7A, B). Survival analysis using TCGA data showed that high expression of these genes was associated with worse outcomes in OS, DFS, and DSS, with low-expression groups having better prognosis (Fig. 7C).

A nomogram model combining CHMP2 A, CHMP4B, age, and gender was constructed to predict 1-year, 3-year, and 5-year survival probabilities, and its accuracy was validated with a calibration curve (Fig. 7D, E). Risk ratio analysis indicated that high expression of CHMP2 A and CHMP4B was closely related to poor prognosis (Fig. 7F). Further analysis showed that CHMP4B expression was significantly higher in tumor tissues than in normal tissues, and its

Fig. 6 Expression and prognosis analysis of key pyroptosis-related genes.**A**: Violin plot of differential expression of key pyroptosis-related genes in TCGA and GEO datasets.**B**: Violin plot of ssGSEA scoring results.**C**: Line chart of score changes in patients with different clinical stages.**D**: KM curve for patients with high and low pyroptosis risk groups.**E**: KM curve for patients in the GEO external validation set with high and low pyroptosis risk groups.**F**: KM curve for patients in the ICGC external validation set with high and low pyroptosis risk groups.**G**: Identification of malignant, mixed, and normal cells in spatial transcriptomic data.**H**: Activity landscape of key pyroptosis-related genes in microregions.**I**: Differences in AUC scores of key pyroptosis-related genes in malignant, mixed, and normal microregions under spatial transcriptomic resolution.**J**: Spearman correlation of pyroptosis key gene AUC scores with microenvironment components.**K**: GO enrichment analysis for patients in high and low pyroptosis groups.**L**: GSEA enrichment of Hallmark gene sets in high and low pyroptosis groups

expression increased as liver cancer progressed (Fig. 7G-J). Meta-analysis further confirmed the prognostic value of CHMP2 A and CHMP4B across various survival metrics (Fig. 7L).

3.8 CHMP4B Expression and Immune Infiltration

We further explored the relationship between CHMP4B expression, immune infiltration, prognosis, and functional enrichment in liver cancer. Survival analysis (Fig. 8A, B) indicated that high CHMP4B expression was associated with significantly shorter OS and poorer prognosis. Spatial transcriptomic analysis (Fig. 8C) revealed heterogeneous CHMP4B expression in the tumor microenvironment. Immune infiltration analysis (Fig. 8D) showed that high CHMP4B expression was correlated with increased infiltration of immune cells, such as monocytes, macrophages, and T cells. Correlation analysis (Fig. 8E-G) further demonstrated that high CHMP4B expression was positively correlated with immune checkpoint molecules (e.g., PD-L1, CTLA4), suggesting its role in promoting immune evasion.

Gene correlation analysis (Fig. 8H) and tumor microenvironment analysis (Fig. 8I) supported the finding that immune-suppressive cells were more prevalent in the high CHMP4B expression group. Functional enrichment analysis (Fig. 8J, K) indicated that high CHMP4B expression was closely associated with pathways involved in cell cycle, DNA repair, and cytoskeletal organization. These results suggest that high CHMP4B expression is not only linked to poor prognosis in liver cancer patients but may also promote cancer progression by regulating immune suppression and the tumor microenvironment, making it a potential therapeutic target and prognostic biomarker.

3.9 Validation of CHMP4B expression by experiment

The Fig. 9 results showed that CHMP4B expression levels were significantly higher in liver cancer tissues compared to normal liver tissues. Both the HepG2 ($p < 0.05$) and the Huh7 ($p < 0.01$) exhibited statistically significant differences. Analysis using GraphPad Prism software indicated that CHMP4B expression was upregulated in liver cancer tissues, suggesting its potential role in liver cancer development and progression. Experimental data were presented as mean ± standard error (Mean ± SEM), and differences between groups were statistically analyzed using one-way ANOVA, with $p < 0.05$ considered statistically significant. In conclusion, the qRT-PCR results suggest that CHMP4B expression is significantly increased in liver cancer tissues and may play an important role in the progression of liver cancer.

4 Discussion

Pyroptosis is a form of programmed cell death that has been extensively studied in recent years. It is characterized by the activation of inflammasomes and caspase family proteins, leading to membrane rupture and the release of intracellular contents, which triggers a strong inflammatory response [18, 19]. Unlike apoptosis, which is typically associated with minimal immune stimulation, pyroptosis induces a more potent immune response, potentially playing a crucial role in anti-tumor immunity. However, pyroptosis is not limited to anti-tumor effects; in certain contexts, it may also promote tumor development [20, 21]. Tumor cells, by regulating pyroptosis-related genes, can alter the tumor microenvironment, facilitating immune evasion and even enhancing tumor aggressiveness. Through machine learning-based analysis, we identified CHMP4B as a key pyroptosis-related gene in hepatocellular carcinoma (HCC). Survival analysis revealed that high CHMP4B expression is significantly associated with poor prognosis in HCC patients, particularly in terms of overall survival (OS) and disease-free survival (DFS) [22]. Pyroptosis-related genes, through inflammasome activation, trigger a cascade of inflammatory reactions that can impact immune cell behavior within the tumor microenvironment. While inflammation typically aids in clearing tumor cells, chronic inflammation in the tumor microenvironment may selectively activate immunosuppressive cells and molecules, thereby promoting tumor growth and progression [22].

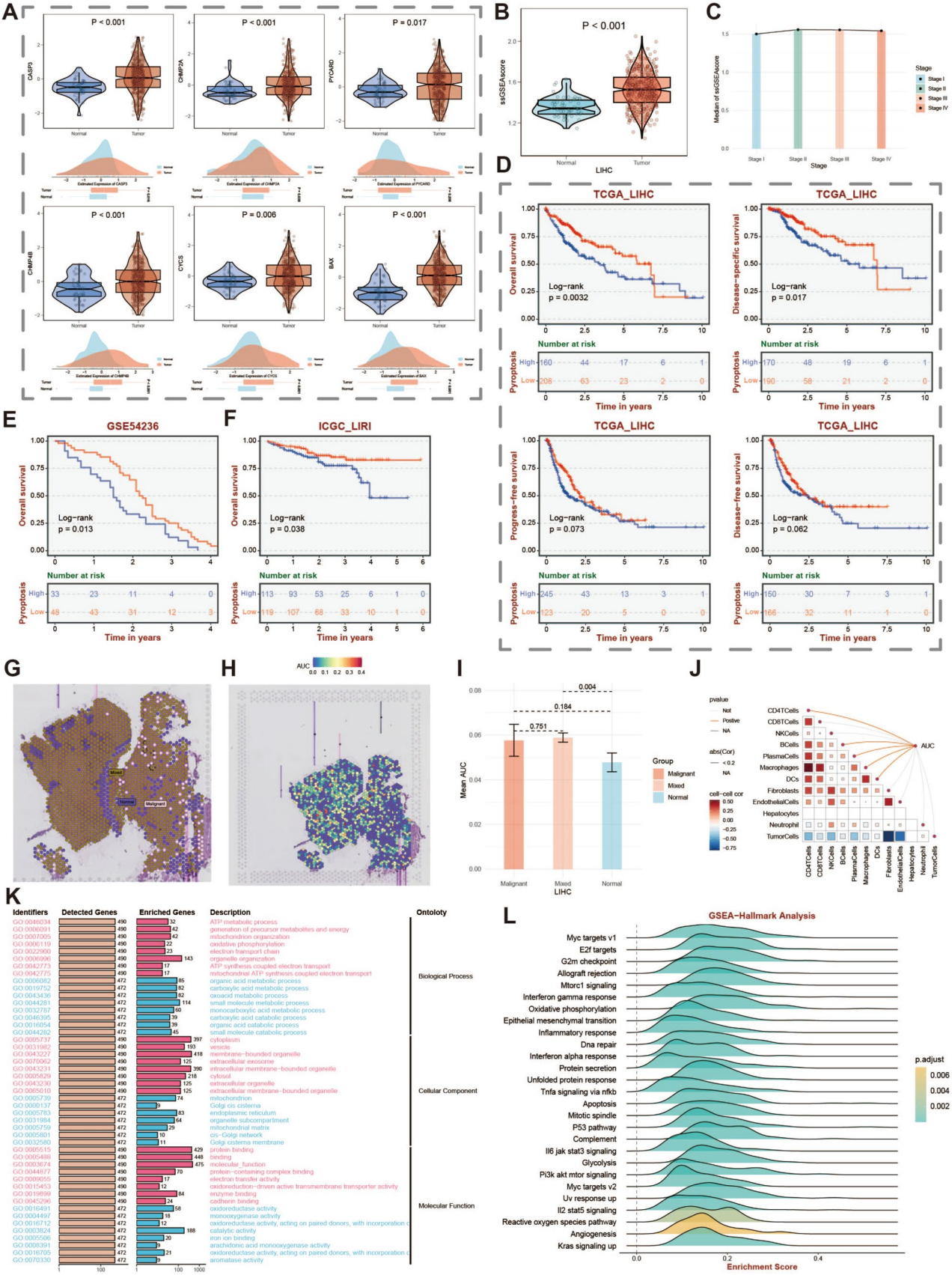
A
P < 0.001
P < 0.001
P = 0.017
P < 0.001
P = 0.006
P < 0.001
Normal
Tumor
B
P < 0.001
ssGSEAscore
LIHC
C
Median of ssGSEAscore
Stage
Stage I
Stage II
Stage III
Stage IV
D
TCGA_LIHC
Overall survival
Log-rank p = 0.0032
Disease-specific survival
Log-rank p = 0.017
Progress-free survival
Log-rank p = 0.073
Disease-free survival
Log-rank p = 0.062
Number at risk
Pyroptosis
High
Low
Time in years
E
GSE54236
Log-rank p = 0.013
F
ICGC_LIRI
Log-rank p = 0.038
G
Mixed
Normal
Malignant
H
AUC
I
Mean AUC
0.004
0.184
0.751
Group
Malignant
Mixed
Normal
LIHC
J
pvalue
Not
Postive
NA
abs(Cor)
< 0.2
cell−cell cor
CD4TCells
CD8TCells
NKCells
BCells
PlasmaCells
Macrophages
DCs
Fibroblasts
EndothelialCells
Hepatocytes
Neutrophil
TumorCells
AUC
K
Identifiers
Detected Genes
Enriched Genes
Description
Ontology
Biological Process
Cellular Component
Molecular Function
L
GSEA−Hallmark Analysis
Myc targets v1
E2f targets
G2m checkpoint
Allograft rejection
Mtorc1 signaling
Interferon gamma response
Oxidative phosphorylation
Epithelial mesenchymal transition
Inflammatory response
Dna repair
Interferon alpha response
Protein secretion
Unfolded protein response
Tnfa signaling via nfkb
Apoptosis
Mitotic spindle
P53 pathway
Complement
Il6 jak stat3 signaling
Glycolysis
Pi3k akt mtor signaling
Myc targets v2
Uv response up
Il2 stat5 signaling
Reactive oxygen species pathway
Angiogenesis
Kras signaling up
p.adjust
Enrichment Score

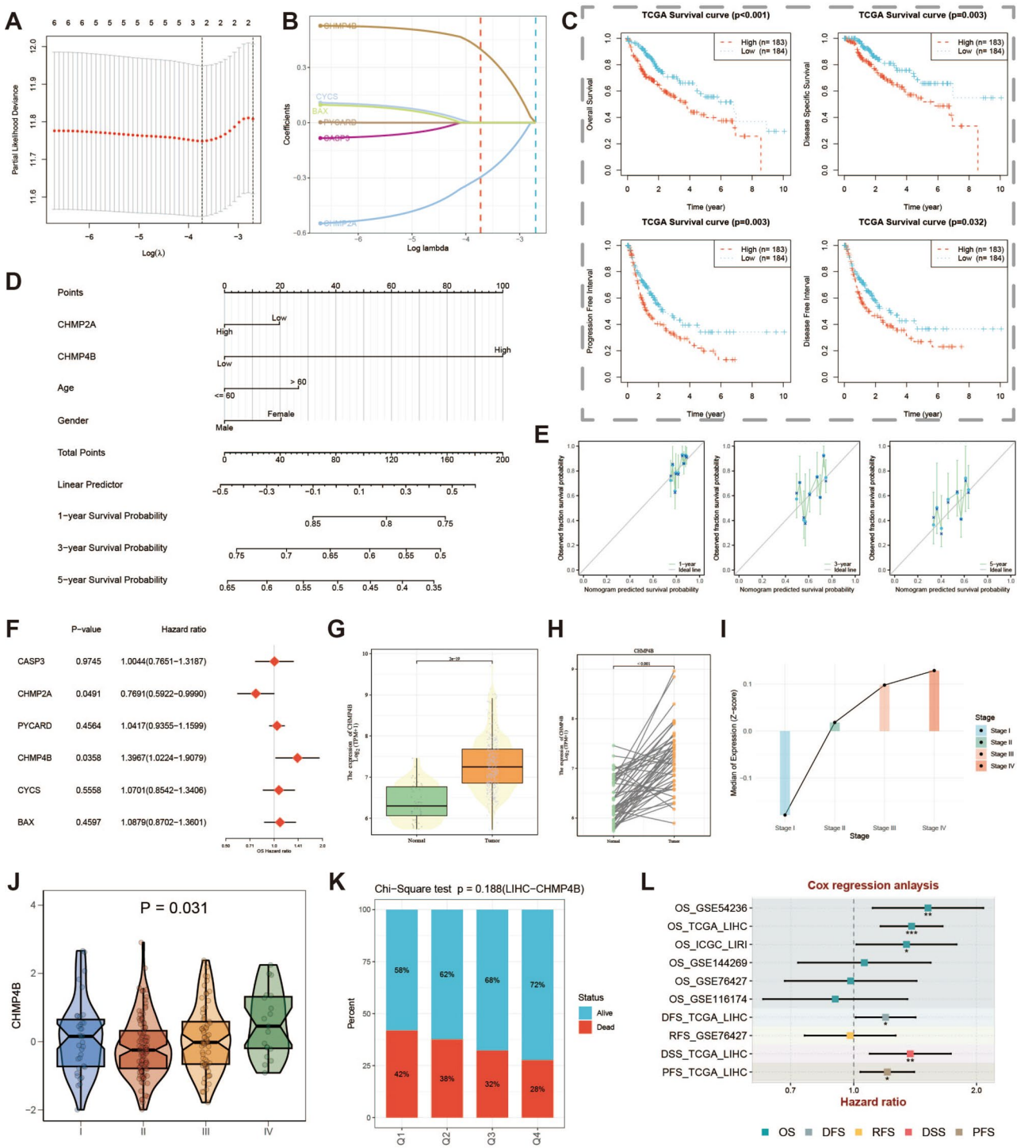

Fig. 7 Prognostic model related to pyroptosis.**A**: Ten-fold cross-validation results.**B**: Lasso regression coefficient path plot.**C**: KM curves for patients with high and low risk, showing overall survival, disease-specific survival, disease-free survival, and progression-free survival.**D**: Nomogram of prognostic marker genes and clinical traits.**E**: Calibration curves for 1-, 3-, and 5-year survival.**F**: Forest plot of key pyroptosis-related genes.**G**: Box plot of CHMP4B expression levels.**H**: Line chart of CHMP4B expression in paired samples.**I**: Line chart of CHMP4B changes in patients at different clinical stages**J**: Violin plot of CHMP4B changes in patients at different clinical stages.**K**: Kaplan–Meier survival analysis of DSS for patients divided into four groups (Q1, Q2, Q3, Q4) based on CHMP4B expression levels.**L**: Forest plot of CHMP4B risk

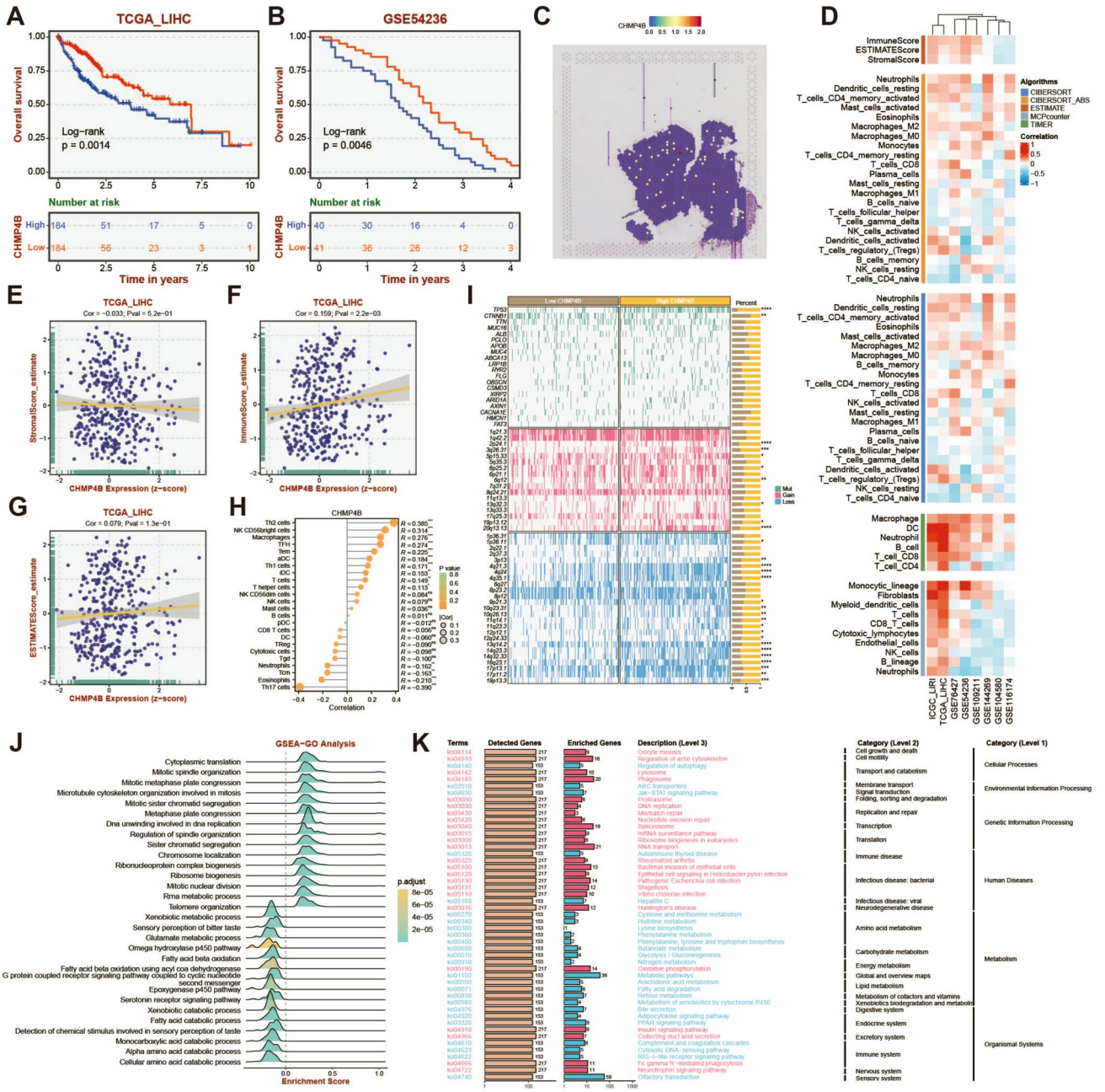

Fig. 8 Prognosis analysis of CHMP4B gene.**A**: KM curve of patient groups based on CHMP4B expression levels**B**: KM curve of patient groups in the GEO external validation set based on CHMP4B expression levels.**C**: Heatmap of CHMP4B expression levels in spatial transcriptomic slice data.**D**: Heatmap of correlations between CHMP4B expression levels and immune cell infiltration.**E–G**: Correlation plots of CHMP4B expression levels with infiltration levels.**H**: Divergent bar chart of correlation between CHMP4B expression levels and immune cell infiltration.**I**: Heatmap of genomic alterations.**J**: Ridge plot of GSEA enrichment results for GO gene sets.**K**: Bar chart of KEGG enrichment analysis results

High CHMP4B expression was closely associated with the infiltration of immunosuppressive cells (e.g., monocytes, macrophages, and T cells) in the tumor microenvironment. It also correlated positively with the expression of immune checkpoint molecules (e.g., PD-L1, CTLA4), suggesting that CHMP4B may establish an immunosuppressive environment that supports tumor survival and growth by triggering abnormal inflammatory responses. Additionally, CHMP4B may promote immune evasion, further driving tumor progression. Spatial transcriptomics analysis revealed heterogeneous CHMP4B expression in the tumor microenvironment, while functional enrichment analysis showed that this gene is involved in various tumor-related biological processes and signaling pathways, including cell cycle regulation, DNA

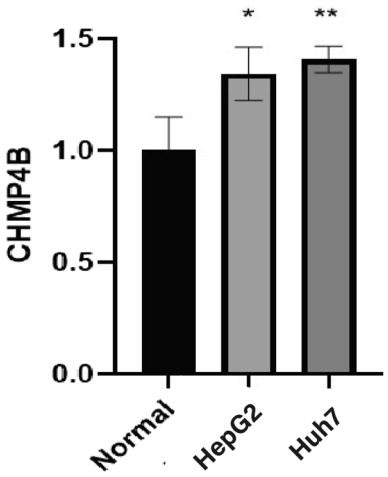

Fig. 9 Validation of CHMP4B expression by PCR

repair, and immune modulation. Moreover, CHMP4B expression increased with tumor stage progression, indicating its crucial role in advanced HCC. Collectively, these findings suggest that CHMP4B plays a pivotal role in HCC prognosis, immune evasion, and tumor progression, making it a potential target for clinical applications [23].Our functional enrichment analysis demonstrated that CHMP4B overexpression was significantly associated with pathways related to the cell cycle. This finding indicates that pyroptosis-related genes may play a key role in regulating tumor cell proliferation and division [24]. Aberrant activation of pyroptosis genes can disrupt cellular homeostasis, potentially driving rapid tumor cell growth and malignant transformation. Specifically, CHMP4B may regulate membrane dynamics and intracellular vesicle trafficking, thereby influencing cell cycle regulation and enhancing the proliferative capacity of tumor cells. Furthermore, CHMP4B is closely related to cytoskeleton-associated biological processes, which may suggest its role in tumor cell migration and invasion. Pyroptosis gene activation may alter tumor cell morphology and promote cytoskeletal reorganization, enhancing the invasiveness and metastatic potential of cancer cells. This mechanism may explain why patients with high CHMP4B expression exhibit poorer clinical outcomes, especially in late-stage cancers, where CHMP4B expression is significantly elevated, highlighting its critical role in maintaining the malignant phenotype of tumors [25, 26].

Despite revealing the critical impact of pyroptosis on HCC, our study has some limitations. First, the limited sample size may affect the generalizability of our results. We look forward to future studies involving larger sample sizes and single-cell data from different databases to provide a more comprehensive analysis of the impact of pyroptosis on the HCC tumor microenvironment. Additionally, future research should incorporate multi-omics approaches, such as proteomics and metabolomics, to further elucidate the functional role of CHMP4B and provide a more holistic understanding of its impact on HCC [27–29].

5 Conclusions

Our findings highlight CHMP4B as a critical regulator of pyroptosis in HCC, influencing tumor progression and immune modulation. High CHMP4B expression may facilitate the development of an immunosuppressive microenvironment, enabling immune escape and tumor growth. The study underscores CHMP4B's potential as a prognostic biomarker and therapeutic target in HCC. However, the limited sample size calls for further validation using larger datasets and multi-omics approaches, such as proteomics and metabolomics, to fully elucidate its functional role in HCC pathogenesis.

Acknowledgements We thank Sichuan Dongying Xinda Science and Technology Co. for the help of bioinformatics analysis.

Author contributions YY collected the data. ST and YY wrote the manuscript and analyzed the data. ST and YY designed the research study. All authors approved the final version of the manuscript.

Funding This study was not funded.

Data availability All original data for this paper was obtained from TCGA and GEO public databases and all original data and documents can be found.

Declarations

Competing interests The authors declare no competing interests.

Open Access This article is licensed under a Creative Commons Attribution-NonCommercial-NoDerivatives 4.0 International License, which permits any non-commercial use, sharing, distribution and reproduction in any medium or format, as long as you give appropriate credit to the original author(s) and the source, provide a link to the Creative Commons licence, and indicate if you modified the licensed material. You do not have permission under this licence to share adapted material derived from this article or parts of it. The images or other third party material in this article are included in the article's Creative Commons licence, unless indicated otherwise in a credit line to the material. If material is not included in the article's Creative Commons licence and your intended use is not permitted by statutory regulation or exceeds the permitted use, you will need to obtain permission directly from the copyright holder. To view a copy of this licence, visit http://creativecommons.org/licenses/by-nc-nd/4.0/.

References

1. Tang J, Li S, Zhou Z, Wang Y, Ni D, Zhou S. MiR-3680–3p is a novel biomarker for the diagnosis and prognosis of liver cancer and is involved in regulating the progression of liver cancer. IUBMB Life. 2024. https://doi.org/10.1002/iub.2856.
2. Adugna A. Histomolecular characterisation of hepatitis B virus induced liver cancer. Rev Med Virol. 2023;33: e2485.
3. Yang Y, Wu QJ, Xie L, Chow WH, Rothman N, Li HL, Gao YT, Zheng W, Shu XO, Xiang YB. Prospective cohort studies of association between family history of liver cancer and risk of liver cancer. Int J Cancer. 2014;135:1605–14.
4. Maki H, Hasegawa K. Advances in the surgical treatment of liver cancer. Biosci Trends. 2022;16:178–88.
5. Zhang Y, Xiao B, Yuan S, Ding L, Pan Y, Jiang Y, Sun S, Ke X, Cai L, Jia L. Tryptanthrin targets GSTP1 to induce senescence and increases the susceptibility to apoptosis by senolytics in liver cancer cells. Redox Biol. 2024;76: 103323.
6. Singal AG, Hoshida Y, Pinato DJ, Marrero J, Nault JC, Paradis V, Tayob N, Sherman M, Lim YS, Feng Z, Lok AS, Rinaudo JA, Srivastava S, Llovet JM, Villanueva A. International Liver Cancer Association (ILCA) White Paper on Biomarker Development for Hepatocellular Carcinoma. Gastroenterology. 2021;160:2572–84.
7. Mandal SK, Yadav P, Sheth RA. The Neuroimmune Axis and Its Therapeutic Potential for Primary Liver Cancer. Int J Mol Sci. 2024. https://doi.org/10.3390/ijms25116237.
8. Liu ZK, Wu KF, Zhang RY, Kong LM, Shang RZ, Lv JJ, Li C, Lu M, Yong YL, Zhang C, Zheng NS, Li YH, Chen ZN, Bian H, Wei D. Pyroptosis-Related LncRNA Signature Predicts Prognosis and Is Associated With Immune Infiltration in Hepatocellular Carcinoma. Front Oncol. 2022;12: 794034.
9. Li H, Li T, Zhang X. Identification of a pyroptosis-related prognostic signature combined with experiments in Hepatocellular Carcinoma. Front Mol Biosci. 2022;9: 822503.
10. Zou Z, Zhao M, Yang Y, Xie Y, Li Z, Zhou L, Shang R, Zhou P. The role of pyroptosis in hepatocellular carcinoma. Cell Oncol (Dordr). 2023;46:811–23.
11. Cheng Chi, et al. Burning down the house: Pyroptosis in the tumor microenvironment of hepatocellular carcinoma. Life sci. 2024. https://doi.org/10.1016/j.lfs.2024.122627.
12. Tian B, Li Qi. Single-cell sequencing and its applications in liver cancer. Front Oncol. 2022;12(857037):21. https://doi.org/10.3389/fonc.2022.857037.
13. Wang Haiyang, et al. Integrative single-cell transcriptome analysis reveals a subpopulation of fibroblasts associated with favorable prognosis of liver cancer patients". Transl oncol. 2021;14(1):100981. https://doi.org/10.1016/j.tranon.2020.100981.
14. Zhong Jinlin, et al. Identification and validation of a T cell marker gene-based signature to predict prognosis and immunotherapy response in gastric cancer". Scientific Rep. 2023;13(1):21357. https://doi.org/10.1038/s41598-023-48930-8.
15. Hu Jing, et al. Development of a cancer-associated fibroblast-related prognostic model in breast cancer via bulk and single-cell RNA sequencing". BioMed Res Internatl. 2022. https://doi.org/10.1155/2022/2955359.
16. Sun Hanlin, et al. Multi-omics analysis-based macrophage differentiation-associated papillary thyroid cancer patient classifier". TranslatIl Oncol. 2024. https://doi.org/10.1016/j.tranon.2024.101889.
17. Liu Wen, et al. Single-cell and bulk RNA sequencing reveal cancer-associated fibroblast heterogeneity and a prognostic signature in prostate cancer". Medicine. 2023. https://doi.org/10.1097/MD.0000000000034611.
18. Yang Fan, et al. Pyroptosis and pyroptosis-inducing cancer drugs". Acta pharmacol Sinica. 2022;43(10):2462–73. https://doi.org/10.1038/s41401-022-00887-6.
19. Zhang Wenting, et al. Bioorthogonal Disruption of Pyroptosis Checkpoint for High-Efficiency Pyroptosis Cancer Therapy". J Am Chem Soc. 2023;145(30):16658–68. https://doi.org/10.1021/jacs.3c04180.
20. Fang Yuan, et al. Pyroptosis: a new frontier in cancer". Biomed Pharmacother. 2020;121(2020):109595. https://doi.org/10.1016/j.biopha.2019.109595.
21. Xing Yuqi, et al. Augmented antitumor immune responses of HER2-targeted pyroptotic induction by long-lasting recombinant immunopyroptotins". Heliyon. 2024;10(9):e30444. https://doi.org/10.1016/j.heliyon.2024.e30444do.
22. Wang Jiwei, et al. Pyroptosis and the fight against lung cancer". Medl Res Rev. 2024. https://doi.org/10.1002/med.22071.
23. Zhao Pengzhan, et al. Up-regulation of CHMP4B alleviates microglial necroptosis induced by traumatic brain injury". J cell Mol Med. 2020;24(15):8466–79. https://doi.org/10.1111/jcmm.15406.
24. Sagona Antonia P, et al. Association of CHMP4B and autophagy with micronuclei: implications for cataract formation". BioMed Res Internatl. 2014. https://doi.org/10.1155/2014/974393.

25. Hu Baoying, et al. High CHMP4B expression is associated with accelerated cell proliferation and resistance to doxorubicin in hepatocellular carcinoma". Tumour Biol. 2015;36(4):2569–81. https://doi.org/10.1007/s13277-014-2873-1.
26. Wang Mingzhu, et al. BMP4 preserves the developmental potential of mESCs through Ube2s- and Chmp4b-mediated chromosomal stability safeguarding". Protein cell. 2022;13(8):580–601. https://doi.org/10.1007/s13238-021-00896-x.
27. Xu Jiayu, et al. Uncovering the Impact of Aggrephagy in the Development of Alzheimer's Disease: Insights Into Diagnostic and Therapeutic Approaches from Machine Learning Analysis. Current Alzheimer Res. 2023;20(9):618–35. https://doi.org/10.2174/0115672050280894231214063023.
28. Tang Jingyi, et al. Causal relationship between immune cells and hepatocellular carcinoma: a Mendelian randomisation study". J Cancer. 2024;15(13):4219–31. https://doi.org/10.7150/jca.96744.
29. Jiang Lai, et al. Role of glycosylation-related gene MGAT1 in pancreatic ductal adenocarcinoma". Front Immunol. 2024;15:1438935. https://doi.org/10.3389/fimmu.2024.1438935.

Publisher's Note Springer Nature remains neutral with regard to jurisdictional claims in published maps and institutional affiliations.